# Effect of surface morphology on the fracture strength of silicon nanobeams

Cite as: Appl. Phys. Lett. **89**, 091901 (2006); https://doi.org/10.1063/1.2338649
Submitted: 18 April 2006 . Accepted: 03 July 2006 . Published Online: 28 August 2006

Tuncay Alan, Melissa A. Hines, and Alan T. Zehnder

# Effect of surface morphology on the fracture strength of silicon nanobeams

Tuncay Alan,[a] Melissa A. Hines, and Alan T. Zehnder
*Cornell Center for Materials Research, Cornell University, Ithaca, New York 14853*

(Received 18 April 2006; accepted 3 July 2006; published online 28 August 2006)

The effect of nanoscale surface morphology on the fracture strength of 190-nm-thick, doubly clamped Si beams was measured experimentally. The surface morphology was controlled through aqueous etching and characterized by atomic force microscopy. The beams fractured along the primary cleavage planes, {111}. Fracture strength was extracted using finite element simulations of the experiment. Nanobeams etched with relatively smooth morphologies (0.4 nm rms) were able to sustain a tensile stress of 15.8 GPa, close to theoretical strengths predicted by previous atomistic calculations. In contrast, nanobeams decorated with nanometer-high step bunches (1.5 nm rms) had a 20% lower fracture strength, 12.8 GPa, suggesting that careful attention to processing is necessary for maximum strength. © *2006 American Institute of Physics*. [DOI: 10.1063/1.2338649]

Macroscopic materials are typically much weaker than would be predicted from a simple bond strength analysis, since extended defects such as dislocations compromise strength. For example, atomistic calculations considering the cleavage of a perfect Si crystal along a {111} plane predict a tensile strength of 23 GPa and a shear strength of 6.5 GPa,[1] whereas millimeter-size pieces of silicon have a mean strength of only 0.5 GPa.[2] Nanoscale materials, with dimensions close to the characteristic size of intrinsic or process-induced defects (~0.2 nm considering the Griffith fracture criterion[3] and a 23 GPa tensile strength), have the potential to be much stronger. Indeed, the mean strength of silicon increases 35-fold as the length scale changes from millimeters to nanometers.[2] These size-dependent changes in strength are particularly important to commercial microelectromechanical systems (MEMSs), and there has been an ongoing effort to characterize the mechanical properties and fracture reliability of nanoscale structures.[2–6]

Will nanoscale materials ever reach their theoretical strengths or will surface defects, such as process-induced roughness or even atomic steps, always limit performance? To investigate this question, we characterize the fracture strength of 190-nm-thick, H-terminated, single-crystal silicon beams and show that even the small increase in surface roughness (1.5 nm rms) induced by chemical etching significantly reduces fracture strength. This result implies that careful attention to MEMS processing conditions will be necessary to achieve optimum strength and reliability. In addition, these experiments measured fracture along {111} planes, enabling comparison with theoretical calculations.

In continuum mechanics, failure due to stress concentrations is well understood. Brittle solids fail when the applied stress exceeds a critical value, $\sigma_c$. When a rough material is stressed, surface features, such as steps, act as stress concentrators. Extending Williams' notch analysis,[7] at the root of an ideal step, the local stress $\sigma_{\mathrm{loc}}(x) \sim \sigma_g(x)[h(x)/r(x)]^{0.456}$, where $\sigma_g(x)$ is the global stress (in the absence of a notch), $h(x)$ is the height of the step at location $x$, and $r(x)$ is the distance from the step root. This suggests that a 100% increase in the roughness reduces the fracture stress by 35%.

To characterize the effects of nanoscale roughness on silicon samples with well defined morphology, 190-nm-thick, 500-nm-wide, 12-$\mu$m-long doubly clamped suspended beams, such as the one shown in Fig. 1, were fabricated from Si(111) wafers using a previously described procedure.[8] Briefly, the lateral shape of the beams was defined photolithographically, such that the long axis of the beam was parallel to the $[1\bar{1}0]$ direction, then the beam height was established by reactive ion etching (RIE). The wafers were protected by a 100-nm-thick, well annealed thermal oxide, which presumably engulfed any RIE-induced damage, and smoothed the sidewalls. Using a second step of photolithography and RIE, a deep triangular well was defined around (but not under) each beam. The wafer was then diced into conveniently sized samples and stored until needed.

Before each experiment, the sample chip was scrupulously cleaned using a modified RCA clean.[8] The oxide-protected beams were then released from the substrate using one of two highly anisotropic etches that rapidly consumed all non-{111} silicon planes while leaving the protective oxide layer intact. As a result of this anisotropy, the etch self-terminated on the triangular {111} well walls and the beam back sides. Both etches used strong aqueous bases and produced nominally flat, H-terminated Si(111) surfaces. The first etch consisted of a 4 min immersion in 72 °C, 50% *w*/*v*

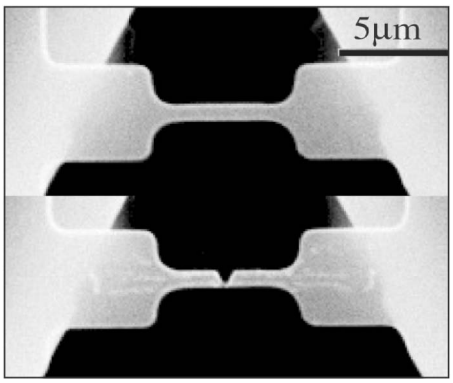


FIG. 1. (a) Silicon beam before the test and (b) fractured silicon beam showing triangular cleavage along {111} planes.

[a]Electronic mail: ta39@cornell.edu

 

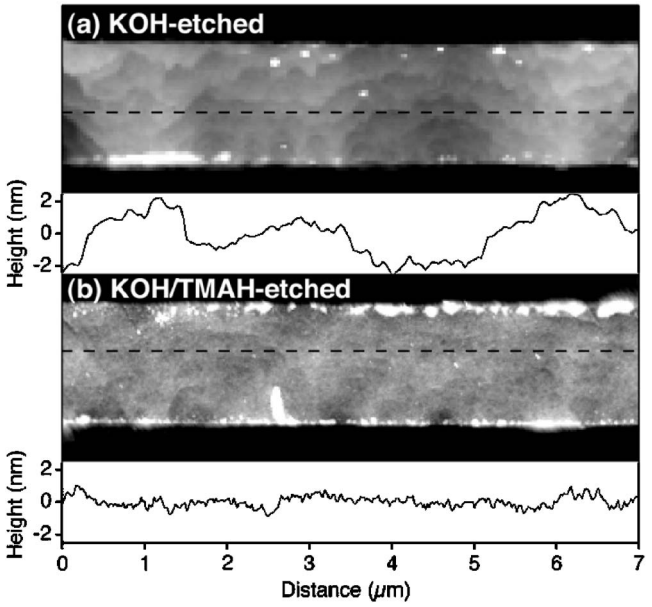


FIG. 2. AFM images and line scans of etched beams. (a) A 4 min KOH etch leads to a macrostepcovered surface (1.5 nm rms), and (b) a 3 min KOH etch followed by a 4 min TMAH etch leads to smooth surfaces (0.4 nm rms).

potassium hydroxide (KOH, Lab Chem); the second etch consisted of a 3 min KOH etch followed by a 4 min immersion in 72 °C, 25% *w*/*w* tetramethylammonium hydroxide (TMAH, Transene). After release, the protective oxide was removed from the top and side surfaces of the beams without further silicon etching using a 2 min immersion in buffered oxide etch [J. T. Baker, a 5:1 mixture of $NH_4F$:HF (aqueous)], which left all surfaces H terminated.

Although chemically similar, the two anisotropic etches produced very different surface morphologies on the unprotected back sides of the beams. To quantify this roughness, we characterized similarly prepared 1.5-$\mu$m-wide beams as shown in Fig. 2. The first etch, KOH, produced atomically smooth Si{111} terraces separated by a-few-nanometer-high step bunches or macrosteps.[9] In contrast, the second etch produced much smoother surfaces with no apparent step bunches, as shown by Fig. 2(b). Surface roughness is often characterized by a single parameter, the root-mean-square (rms) roughness $R_q$; however, we caution that this parameter is relatively insensitive to morphological structure (e.g., step bunches). From atomic force microscopy (AFM) images, the rms roughness of the KOH-etched surfaces was 1.5 nm, whereas the KOH/TMAH-etched surfaces had a 0.4 nm rms roughness.

The final beam thickness was a function of the duration of the first RIE and the nature and duration of the anisotropic etch.[8] To accurately calculate the beam thicknesses, the resonant frequencies of typically prepared beams were measured in vacuum. The measured frequencies were converted to absolute thicknesses by comparison to finite element analysis (FEA) simulations which incorporated the full anisotropy of the Si lattice and known mechanical properties.

An uncoated, stiff, single-crystal Si AFM cantilever (Veeco TAP525) was used to deflect the center of each beam to the point of fracture, as sketched in Fig. 3. The tapered corners of the beam supports prevented unwanted stress concentrations during loading. As a result, the maximum tensile stress was reproducibly located at the center back side of the

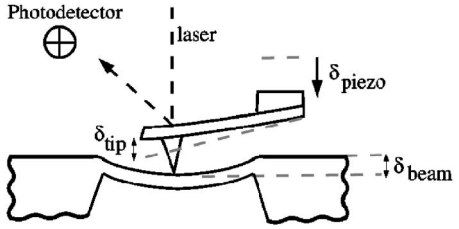


FIG. 3. Schematic of AFM cantilever loading a test beam.

beam, where the surface morphology was well controlled. This control is reflected in the triangular fracture geometry observed in Fig. 1(b), which indicates cleavage along {111} planes. All of the tested beams fractured at the center of the beam and along the primary cleavage planes, {111}. As will be discussed later, this control is crucial for comparisons with theoretical predictions.

The applied force $F$ and the deflection of the beam, $\delta_{\text{beam}}$, during loading were continuously measured as follows. The AFM deflection $\delta_{\text{tip}}$ was first calibrated by monitoring the photodetector signal as the cantilever was pressed against a noncompliant substrate by a known distance, $\delta_{\text{piezo}}$. Using this calibration, the beam deflection could be calculated from $\delta_{\text{beam}}=\delta_{\text{piezo}}-\delta_{\text{tip}}$ as illustrated by Fig. 3. The resonant frequency of the cantilever was measured with the AFM, and the cantilever dimensions and tip position were determined with an optical surface profilometer and a scanning electron microscope. The cantilever thickness was obtained by comparing measured resonance frequencies with FEA simulations. Using these data and a static FEA calculation, the spring constant of the cantilever, $k_{\text{AFM}}$, was calculated. The applied force could then be calculated from $F=k_{\text{AFM}}\delta_{\text{tip}}$. To minimize errors, all of the mechanical tests reported here were performed in a single sitting with the same cantilever.

Because of their high strength, the nanobeams withstood large displacements (approximately five times the beams' thickness) before fracture, as illustrated by the inset in Fig. 4. To rigorously account for the large deflections, the nonuniform width of the beams, and the full anisotropy of the mechanical properties of silicon, a geometrically nonlinear three-dimensional anisotropic FEA was used to extract the

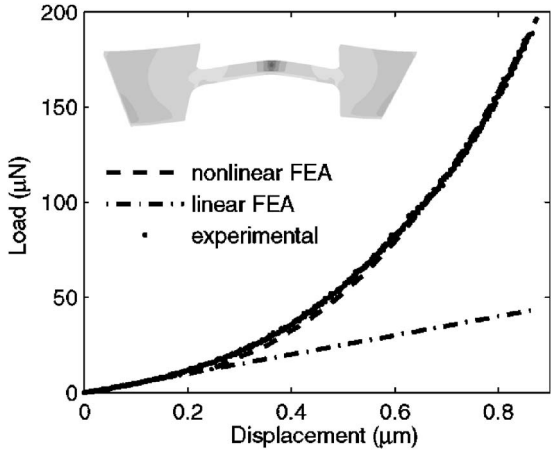


FIG. 4. Comparison of an experimental load-deflection curve with those predicted by linear elastic theory and geometrically nonlinear FEA calculations. Inset: Deformed shape of the test beam at fracture, with colors representing stress levels.

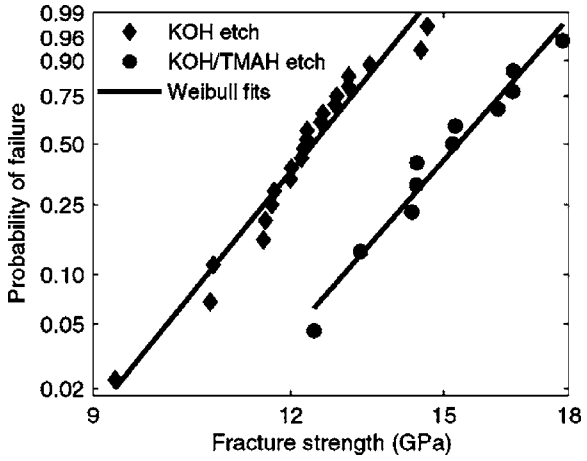


FIG. 5. Weibull failure probability of beams with rough (KOH-etched) and smooth (KOH/TMAH-etched) surfaces. The Weibull parameters $(\sigma_0, \rho)$ are (12.8 GPa, 12.2) and (15.8 GPa, 11.3), respectively.

fracture strength (the maximum tensile stress in the beam-length direction, $[1\bar{1}0]$) from the load applied at the point of failure. (Previous AFM-based measurements of fracture strength[2] have used analytical expressions derived for homogeneous materials in the linear regime.) To demonstrate the accuracy of this procedure, Fig. 4 compares the measured applied force $F$ as a function of deflection to that predicted by both linear beam theory and the geometrically nonlinear FEA simulation.

A perfect, defect-free material would presumably fracture at the same load every time (neglecting the effects of thermal energy.) In contrast, the fracture strength of real (brittle) materials follows a Weibull probability distribution, which models the "weakest link" failure: the whole sample fails when the stress at the weakest link (i.e., surface or volume defect) is exceeded.[10] In our experiments, since defects at the top and side surfaces were minimized, and fracture always occurred at the center, the chemically modified beam back sides were assumed to be the active flaw sites. The probability of failure is a function of the stress $\sigma$ and given by $P_f(\sigma)=1-e^{-(\sigma/\sigma_0)^\rho}$, where $\sigma_0$ is the Weibull strength and $\rho$ is the Weibull shape parameter. The shape parameter controls the width of the fracture distribution, with large scatter corresponding to small $\rho$.

The fracture data for many replicate KOH and KOH/TMAH samples are displayed in Weibull fracture probability plots in Fig. 5. Clearly, the smoother KOH/TMAH-etched beams ($R_q$=0.4 nm) fail at significantly higher loads than the rough, macrostep-covered KOH-etched beams ($R_q$=1.5 nm). The Weibull strengths of these beams are 15.8 and 12.8 GPa, respectively, implying that nanoscale surface roughness can decrease fracture strength by almost 20%. These results also imply that a small change in processing conditions can significantly impact the strength of nanoscale devices. Interestingly, both distributions are characterized by very similar shape parameters. The rough and smooth beams have $\rho$=12.2 and 11.3, respectively, which implies a slightly narrower failure distribution for KOH-etched beams. (This difference may not be statistically significant.)

The well controlled fracture geometry allows for a comparison of the measured fracture strengths with theoretical calculations. On the cleavage plane, the experimentally applied stress has both tensile and shear components. A lower bound for these could be obtained considering perfectly flat surfaces: upon geometric transformations, the 15.8 GPa experimental fracture strength (maximum tensile stress along the $[1\bar{1}0]$ direction) corresponds to a combination of a 7.9 GPa tensile stress normal to {111} planes and a 5.6 GPa shear stress parallel to {111} planes. In comparison, Roundy and Cohen[1] predicted a tensile strength of 23 GPa and a shear strength of 6.5 GPa on {111} planes. Importantly, our smoothest beams, which were produced by KOH/TMAH etching, have strengths very close to the theoretical maximum.

This work was supported by the Cornell Center for Materials Research (CCMR), a Materials Research Science and Engineering Center of the National Science Foundation (DMR-0520404), and performed in part at the Cornell NanoScale Facility, a member of the National Nanotechnology Infrastructure Network which is supported by the National Science Foundation (ECS 03-35765).

[1] M. Roundy and M. L. Cohen, Phys. Rev. B **64**, 212103 (2001).
[2] T. Namazu, Y. Isono, and T. Tanaka, J. Microelectromech. Syst. **9**, 450 (2000).
[3] I. Chasiotis and W. G. Knauss, J. Mech. Phys. Solids **51**, 1533 (2003).
[4] T. Tsuchiya, O. Tabata, J. Sakata, and Y. Taga, J. Microelectromech. Syst. **7**, 106 (1998).
[5] W. N. Sharpe and J. Bagdahn, Mech. Mater. **36**, 3 (2004).
[6] I. Chasiotis and W. G. Knauss, J. Mech. Phys. Solids **51**, 1551 (2003).
[7] M. L. Williams, J. Appl. Mech. **19**, 526 (1952).
[8] Y. Wang, J. A. Henry, A. T. Zehnder, and M. A. Hines, J. Phys. Chem. B **107**, 14270 (2003).
[9] S. P. Garcia, H. Bao, and M. A. Hines, Phys. Rev. Lett. **93**, 166102 (2004).
[10] A. McCarty and I. Chasiotis, Thin Sol. Films (in press).